

# Informing spatial distributions and temporal variations of grass pollen sources in urban landscapes using 10 m Sentinel-2 data

**Yuxia Liu**

Geospatial Science Center of Excellence, Department of Geography and Geospatial Sciences, South Dakota State University <https://orcid.org/0000-0001-6130-2991>

**Alfredo Huete** (✉ [Alfredo.Huete@uts.edu.au](mailto:Alfredo.Huete@uts.edu.au))

School of Life Sciences, Faculty of Science, University of Technology Sydney <https://orcid.org/0000-0003-2809-2376>

**Qiaoyun Xie**

School of Engineering, The University of Western Australia <https://orcid.org/0000-0002-1576-6610>

**Janet M Davies**

School of Biomedical Science, Centre for Immunology and Infection Control and Centre for Environment, Queensland University of Technology <https://orcid.org/0000-0002-6378-4119>

**Paul J Beggs**

Department of Earth and Environmental Sciences, Faculty of Science and Engineering, Macquarie University <https://orcid.org/0000-0001-9949-1783>

**Abolfazl Abdollahi**

Fenner School of Environment & Society, College of Science, The Australian National University <https://orcid.org/0000-0002-1704-4670>

**Biswajeet Pradhan**

Centre for Advanced Modelling and Geospatial Information Systems (CAMGIS), School of Civil and Environmental Engineering, Faculty of Engineering and IT, University of Technology Sydney <https://orcid.org/0000-0001-9863-2054>

**Xiaoyang Zhang**

Geospatial Science Center of Excellence, Department of Geography and Geospatial Sciences, South Dakota State University

---

## Research Article

**Keywords:** Sentinel-2, EVI, ALUM, DLCD, grass map, urban grass pollen, grass pollen sources

**Posted Date:** January 25th, 2024

**DOI:** <https://doi.org/10.21203/rs.3.rs-3894828/v1>

**License:** © ⓘ This work is licensed under a Creative Commons Attribution 4.0 International License.

[Read Full License](#)

**Additional Declarations:** The authors declare no competing interests.

---

# Informing spatial distributions and temporal variations of grass pollen sources in urban landscapes using 10 m Sentinel-2 data

Yuxia Liu<sup>1,2</sup>, Alfredo Huete<sup>1\*</sup>, Qiaoyun Xie<sup>3</sup>, Janet M Davies<sup>4</sup>, Paul J Beggs<sup>5</sup>, Abolfazl Abdollahi<sup>6</sup>, Biswajeet Pradhan<sup>7</sup>, Xiaoyang Zhang<sup>2</sup>

*1 School of Life Sciences, Faculty of Science, University of Technology Sydney, Ultimo, New South Wales 2007, Australia*

*2 Geospatial Science Center of Excellence, Department of Geography and Geospatial Sciences, South Dakota State University, Brookings, SD 57007, USA*

*3 School of Engineering, The University of Western Australia, Perth, WA 6009, Australia*

*4 School of Biomedical Science, Centre for Immunology and Infection Control and Centre for Environment, Queensland University of Technology, Brisbane, Queensland, Australia*

*5 Department of Earth and Environmental Sciences, Faculty of Science and Engineering, Macquarie University, Sydney, New South Wales, Australia*

*6 Fenner School of Environment & Society, College of Science, The Australian National University, Canberra, ACT, Australia*

*7 Centre for Advanced Modelling and Geospatial Information Systems (CAMGIS), School of Civil and Environmental Engineering, Faculty of Engineering and IT, University of Technology Sydney, Ultimo NSW 2007, Australia*

\*Corresponding author.

E-mail address: [Alfredo.Huete@uts.edu.au](mailto:Alfredo.Huete@uts.edu.au)

## Abstract

Grass pollen is a globally prevalent allergen, known to trigger allergic reactions such as hay fever and asthma. Australia, in particular, exhibits one of the highest rates of asthma and hay fever prevalence and morbidity. Accurate mapping of grass pollen sources is crucial for enhancing the capabilities of grass pollen forecast systems. This is especially important in urban landscapes, where the allergenicity associated with urban grass spaces has recently garnered increased attention. However, the spatial distribution of grass in urban landscapes is not well represented in existing coarse-resolution land cover maps. In this study, we evaluated the uncertainties inherent in coarser land cover maps, i.e., Dynamic Land Cover Dataset (DLCD) and Australian Land Use and Management Classification (ALUM) land maps, by comparing them with a 10-m grass map generated from Sentinel-2 data. Subsequently, we characterized the seasonal and inter-annual variations in grass pollen sources surrounding a pollen trap in Sydney, Australia, based on the correlations between the Enhanced Vegetation Index (EVI) of grass and grass pollen concentrations. Our results show that (1) the 10-m Sentinel-2 grass map effectively excludes non-grass features, thereby improving correlation with in-situ grass phenology observations; (2) the correlations between grass EVI, filtered by Sentinel-2 grass map, and grass pollen concentrations varied across different land plots with varied grass fractions, but the grass fraction was not the primary controlling factor; (3) The pollen trap station exhibited significant seasonal and inter-annual variability in grass pollen sources, necessitating further investigation into the meteorological influences on grass phenology and pollen emissions. This study demonstrates the promising performance of Sentinel-2 data in identifying the spatial distribution of grasses, improving the characterization of grass greenness, and mapping grass pollen sources with finer spatial resolution. These findings provide robust data support to enhance our understanding of grass pollen aerobiology in urban areas.

## Keywords

Sentinel-2; EVI; ALUM; DLCD; grass map; urban grass pollen; grass pollen sources

## 1. Introduction

Grass pollen is a major source of airborne allergens, capable of triggering allergic symptoms such as hay fever and asthma (Brennan et al., 2019; Darrow et al., 2012; Devadas et al., 2018; Erbas et al., 2015; Kmenta et al., 2016). In Australia, the prevalence and impact of hay fever and asthma are among the highest globally (Asher et al., 2007), leading to a substantial public health burden associated with allergic respiratory diseases (Davies et al., 2015) and significant government healthcare costs (Beggs et al., 2015). Therefore, it is crucial to enhance the prediction of grass pollen in the environment, particularly in urban regions where the increasing allergenicity is associated with urban green spaces (Cariñanos et al., 2002; De Linares et al., 2010; Rojo et al., 2022).

Satellite-based remote sensing has proven effective in enhancing predictive models of grass pollen aerobiology. It provides valuable information on phenological timing of grass (Descals et al., 2020; Gómez-Giráldez et al., 2020; Vrieling et al., 2018) and enables the mapping of grass spatial distributions (Khwarahm et al., 2016; McInnes et al., 2017; Rapinel et al., 2019; Verstraeten et al., 2021). This technology plays a crucial role in mitigating the health and socioeconomic impact of allergic diseases caused by grass pollen sensitivity.

Maps showing the locations of allergenic vegetation taxa have been adopted in various application scenarios, including combining with weather data to improve pollen forecasting (Zink et al., 2011); combining with health data to inform exposure of aeroallergens (Newson et al., 2014); improving pollen emission models (Zink et al., 2013); and enhancing individuals' self-management of allergy or asthma (McInnes et al., 2017). Vegetation mapping of plants with allergenic pollen requires land cover maps as the reference (i.e., base maps). For example, using the Corine Land Cover 2000 (CLC2000) (100 m) as a base map, Khwarahm et al. (2016) mapped the birch and grass pollen seasons in the UK. Similarly, finer resolution satellite data (Quickbird satellite images) was combined with the CLC2000 land cover map to derive grass pollen sources across the city of Aarhus, Denmark (Skjøth et al. 2013). Another land cover map with a 25m spatial resolution (Centre for Ecology and Hydrology (CEH) Land Cover Map 2007) was used to generate a grass map in the UK (McInnes et al., 2017). In contrast to the northern hemisphere, studies of allergenic grass pollen sources in Australia have remained reliant on coarse spatial resolution land cover maps, such as the International Geosphere-Biosphere Programme (IGBP, 500m) land classification system (Devadas et al., 2018) or Australian Land Use and Management Classification (ALUM, 50m) (Emmerson et al., 2019). Although the Dynamic Land Cover Dataset (DLCD, 250m) provided nationally consistent land cover information for Australia, its spatial resolutions cannot meet the requirement for mapping precise grass pollen sources, especially considering the intensive spatial heterogeneity around capital cities and the existence of urban 'green spaces', which play a significant role in grass pollen exposure (Skjøth et al., 2013).

Besides geospatial landscape information on allergenic plants, satellite data can contribute to the retrieval of key phenology timing of allergenic vegetation to better inform pollen aerobiology dynamics and map pollen sources. Utilizing time series of satellite data, previous studies adopted the onset of flowering as the phenological proxy to map allergenic birch pollen sources (Karlsen et al., 2009; Khwarahm et al., 2016). The underlying logic behind using flowering phenophase to interpret pollen seasonal dynamics is the good correlations between timings of birch male flowering and leaf budburst, with only 1.1 day intervals between each other (Linkosalo 1999, 2000). Furthermore, the timing of these two phenophases appears to be closely synchronized with pollen release (Newnham et al., 2013). However, this approach is not suitable for mapping grass pollen sources. Compared to birch (regarded as the major allergenic pollen source in Europe), the flowering time of grass is hard to detect from satellite images due to their tiny flowers. Additionally, Devadas et al. (2018) reported that Australian grass pollinating periods are less synchronous with satellite greenness measures compared with French sites, partly due to the more heterogeneous landscapes and complex species diversity in Australian grasslands (e.g., the co-existence of exotic and native species; see Watson et al., 2019).

Recently, Sentinel-2 satellite data at 10 m resolution has shown potential for generating more precise and updated land cover maps (Chen et al., 2015). The Sentinel-2 satellite was launched when many advanced classification methods based on machine learning approaches were already developed (Phiri et al., 2020). Advanced machine learning techniques such as Random Forests (RF) (Clark 2017; Fragoso-Campón et al., 2018), Support Vector Machines (SVM) (Denize et al., 2018; Nguyen et al., 2020) and Convolutional Neural Network (CNN) (Långkvist et al., 2016; Qiu et al., 2020) have been applied for land cover classification — including crop (Mazzia et al., 2020), forest (Miranda et al., 2019) and grassland (Pelletier et al., 2019; Dewi and Chen 2019) — based on Sentinel-2 data. For example, Segal-Rozenhaimer et al. (2020) applied CNN to classify land cover and obtained a 91% classification accuracy. Based on Sentinel-2 images, scientists adopted three widely used machine learning approaches (RF, Recurrent Neural Network (RNN) and Temporal Convolutional Neural Networks (TempCNN)) to classify the land cover in Victoria, Australia, and achieved high overall accuracies of 94.0%, 90.8% and 94.5%, respectively (Charlotte et al., 2019). Despite the superior 10 m resolution offered by Sentinel-2 imagery-based land cover maps compared to traditional land cover products, there is a notable absence of applications that have employed these maps as a fundamental information for mapping grass pollen sources.

In this study, we employed Sentinel-2 data to gather geospatial and phenological information on grass in urban landscapes, aiming to understand the spatial distributions and temporal variations of grass pollen sources. By examining the correlations between grass pollen concentrations and grass greenness (quantified by the Enhanced Vegetation Index, EVI), we characterized the seasonal and inter-annual spatial variations in potential grass pollen sources surrounding a pollen trap station in Sydney, Australia. The study focused on three primary objectives: (1) quantifying the discrepancies in

filtering grass distributions between the 10-m Sentinel-2 grass map and coarser grass maps within urban landscapes; (2) investigating the consistency and variations in the temporal relationships between grass greenness and grass pollen concentrations at different distances and orientations surrounding the pollen trap station; and (3) characterizing the seasonal and inter-annual variations in the spatial distribution of potential grass pollen sources around the pollen trap station.

## 2. Methods

### 2.1 Site description

This study was conducted at two sites near Sydney and Brisbane (Fig. 1). The Campbelltown pollen station (34.0666 S, 150.7956 E) is located on the TAFE New South Wales campus near Campbelltown City, situated 53 km southwest of Sydney's central business district. According to the latest census of population, there were 169,572 people in the Campbelltown suburb and Local Government Area (<https://www.abs.gov.au/census>). At this site, a phenocam and a pollen trap are collocated to record grass growth and grass pollen information. To compare the performance of filtering grass information across multiresolution grass maps, we conducted this analysis at another phenocam site with urban landscapes, the Rocklea phenocam site (27.5358 S, 152.9934 E), located approximately 9 km south of Brisbane, Queensland.

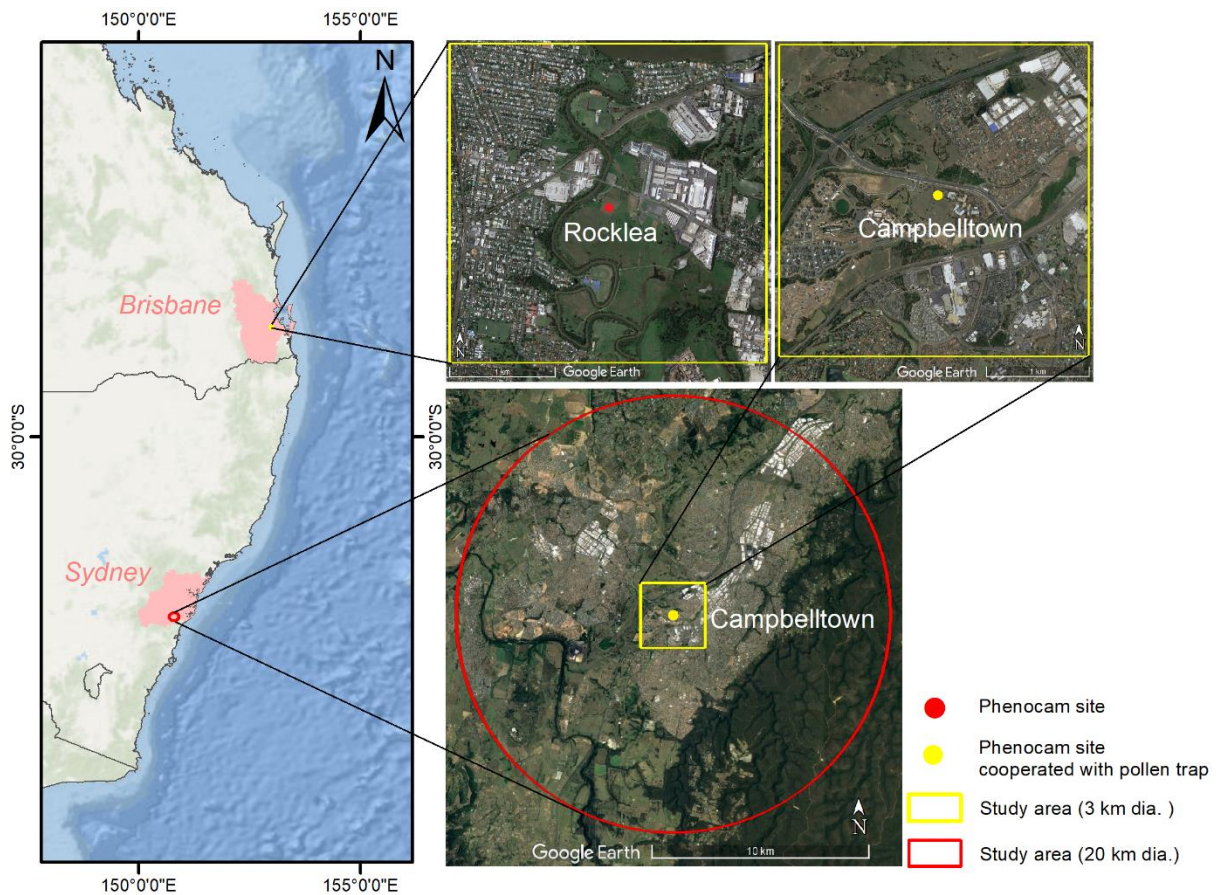


**Fig. 1.** Locations of Campbelltown and Rocklea sites in Sydney and Brisbane. Red circular and yellow squares denote regions where conducted analyses in this study. Google Earth Pro provides the base map.

## 2.2 Multi-resolution grass maps

The Dynamic Land Cover Dataset Version 2 (DLCDv2.1) (<http://www.ga.gov.au/scientific-topics/earth-obs/accessing-satellite-imagery/landcover>) with a spatial resolution of 250 meters was utilized to extract grass greenness information from the landscape in this study. The latest version (updated until the end of 2015) consists of 14 maps, each based on two years of MODIS (Moderate Resolution Imaging Spectrometer) EVI time-series data. These 14 maps cover the period from January 2001 to December 2015. For this study, we specifically used the land cover map for the period of January 2014 to December 2015. Subsequently, we generated a grass map referred to as the DLCD grass map by compositing six original land cover types related to grass/ pasture, including Rain-fed pasture, Closed Tussock Grassland, Open Tussock Grassland, Open Hummock Grassland, Scattered Shrubs, and Grass and Irrigated pasture.

Additionally, we employed the Australian Land Use and Management (ALUM) Classification version 8 (<https://www.agriculture.gov.au/abares/aclump/land-use/alum-classification>) to generate another grass map referred to as the ALUM grass map. The ALUM Classification system offers a nationally consistent method for collecting and presenting land use information at a 50-meter resolution. The current version of this map was developed by the ALUM Classification Technical Working Group in 2016. In our study, the ALUM grass map was generated by combining original land use classes related to grass/ pasture, including Native/exotic pasture mosaic, Grazing irrigated modified pasture & Grazing modified pastures, Pasture legume, and Pasture legume/grass mixtures. Note that other original classes also include grass; for example, Recreation and culture, Services, and Public Services classes typically encompass public green space and grass lawns to varying extents in urban area. We included the Recreation and culture class in the ALUM grass map, as it exhibited the highest grass proportion among these three classes upon visual inspection.

In addition, we utilized a Sentinel-2 grass map with 10-m resolution to enhance our understanding of grass cover in the heterogeneous landscape surrounding the Campbelltown and Rocklea sites. At the Campbelltown site, the Sentinel-2 grass map was generated using a deep learning-based algorithm (the LeNet model) applied to Sentinel-2 images (Abdollahi et al., 2022). The LeNet classification model was trained with 8929 grass samples (i.e., 8929 Sentinel-2 grass pixels) to create a grass map for a  $20 \times 20$  km<sup>2</sup> area centered on the Campbelltown site. To ensure the accuracy of the grass map, all Sentinel-2 grass pixels were selected through visual inspection from Google Earth imagery. As a result, the LeNet model achieved a precision rate of 85.27% for grass classification. Specific details regarding the classification process and results can be found in Abdollahi et al. (2022). Meanwhile, at

the Rocklea site, we manually identified grass pixels from Sentinel-2 imagery based on visual inspection of Google Earth imagery to generate another Sentinel-2 grass map.

### 2.3 Grass greenness proxy and grass pollen concentration data

Enhanced Vegetation Index (EVI) of grass cover was extracted from Sentinel-2 L2A (Level-2A) surface reflectance images, which were masked by multi-resolution grass maps to serve as the proxy for grass greenness for further quantify analyses. The spatial and temporal changes in grass growth during different seasons were determined using Sentinel-2 EVI images. Specifically, all cloud-free Sentinel-2A/B L1C (Level-1C) product over research areas from January 2018 to June 2020 were downloaded. These products were atmospherically corrected from Top-of-Atmosphere (TOA) L1C product to generate L2A surface reflectance product using the Sen2Cor processor (Louis et al., 2016). The L2A outputs were then resampled to a spatial resolution of 10 meters for all bands. Subsequently, EVI was calculated as follows:

$$EVI = 2.5 \times \frac{(NIR-Red)}{(NIR+6 \times Red-7.5 \times Blue+1)} \quad (1)$$

where *NIR*, *Red* and *Blue* represent near-infrared, red and blue bands in terms of the L2A surface reflectance product. The EVI is characterised by an improved sensitivity in high biomass regions and enhanced vegetation monitoring ability through correcting for atmospheric influence and de-coupling of the canopy background signal (Huete et al., 2002).

Two digital time-lapse cameras, known as phenocam, were set up at the Campbelltown and Rocklea sites. They collected digital photos with a time interval of 15 minutes to record variations in the greenness of local grass patches. To quantitatively describe the changes in grass greenness, the green chromatic coordinate (GCC) was derived from phenocam images. Specifically, the region of interest (ROI) was selected from phenocam imagery for each site (Fig. 2); and then RGB DNs (digital number of red, green, and blue channels) for each pixels within the ROI were extracted and converted to GCC by Eq. (2); the GCC value for each pixel was averaged across the ROI to quantify the changes in greenness.

$$GCC = \frac{G}{R+G+B} \quad (2)$$

where *R*, *G* and *B* represent red, green and blue pixel digital numbers.

A grass pollen trap is co-located with the phenocam at the Campbelltown site. Daily (24-hour period) atmospheric grass pollen concentration (grains/m<sup>3</sup>) was collected from January 2018 to June 2020 using Hirst-type volumetric pollen and spore traps (Burkard Scientific Ltd, Uxbridge, UK). Further details on this collection method can be found in Haberle et al. (2014).

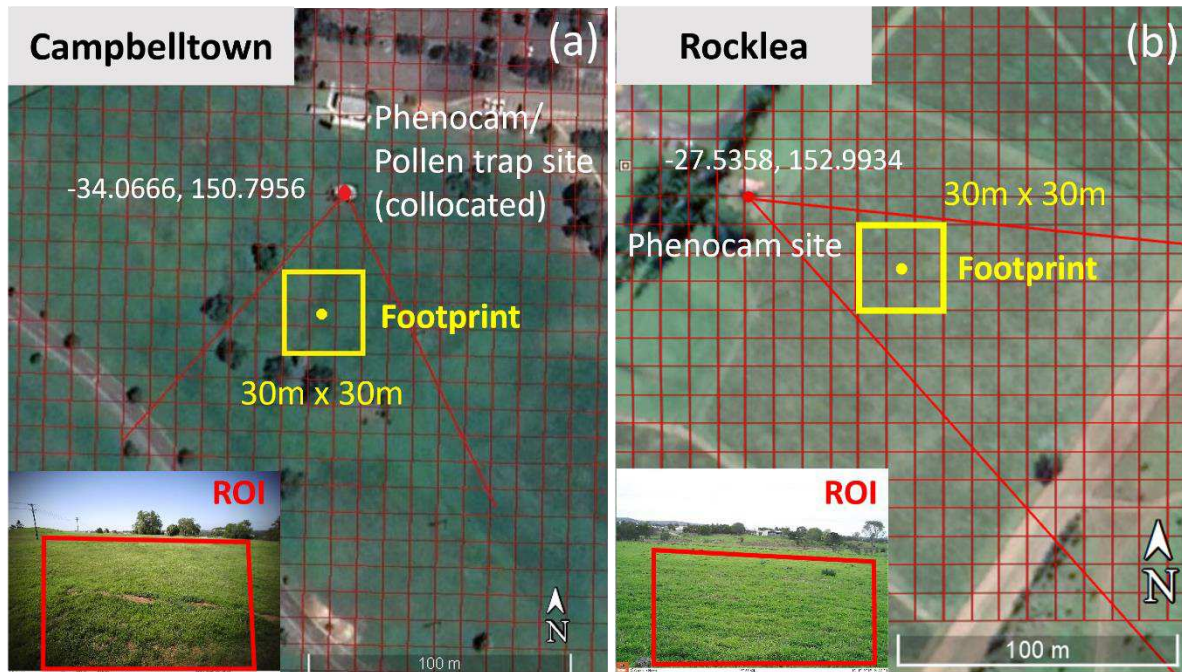


**Fig 2.** Footprint of phenocam ROI (region of interest) in Google Earth images and phenocam sample images in Campbelltown (a) and Rocklea (b) sites. The red grids in Google Earth images are Sentinel-2 pixels with 10 m resolution. The red points are the locations of phenocams and pollen trap. The  $3 \times 3$  Sentinel-2 pixels (yellow squares) depicted the footprint of phenocam ROI, which highlighted by red rectangles in sample phenocam images.

#### 2.4 Analysis strategies

First, we conducted qualitative and quantitative analyses to examine the disparities in grass classification among different grass maps. Specifically, we compared the spatial distribution of grass covers that were identified by Sentinel-2 grass map, ALUM, and DLCD within the  $3 \times 3$  km<sup>2</sup> research area surrounding Campbelltown and Rocklea sites (yellow squares in Fig. 1). Additionally, we compared the number of grass pixels filtered by each grass map. Furthermore, we analyzed the temporal profiles. We also study the correlations between the phenocam GCC and the average grass Sentinel-2 EVI across the entire research area.

Second, we divided the  $20 \times 20$  km<sup>2</sup> circular region surrounding Campbelltown pollen station into 40 land plots (red circle in Fig. 1). These land plots were categorized based on five distance ranges (2 km – 10 km, with intervals of 2 km) and eight orientations (every 45° from 0° – 360°). The Sentinel-2 grass EVI (hereinafter: grass EVI), filtered by Sentinel-2 grass map, were averaged from each land plot. To temporally align grass pollen data with grass EVI, we correlated five-day mean grass pollen concentrations (i.e., mean value for  $\pm 2$  days of the date for the given Sentinel-2 EVI) with grass EVI in each land plot. Note that the correlation analysis was conducted by least-squares linear regression analyses with quadratic parameter to determine the coefficients of determination ( $R^2$ ), since simple

linear regression cannot adequately fit the curvilinear relationship between grass pollen concentrations and grass EVI. Furthermore, we explored the impact of grass fractions on the correlations between grass EVI and grass pollen concentrations (hereinafter: grass EVI – pollen correlations).

Third, pixel-wise grass source maps for each grass pollen season were generated by examining the correlations between time series of grass EVI and grass pollen concentrations. Specifically, grass pollen seasons were defined based on the time series of grass pollen concentrations and average grass EVI in the  $20 \times 20 \text{ km}^2$  region. Using the  $R^2$  values of correlations between time series of grass EVI and five-day mean grass pollen concentration for each pixel, we mapped pixel-wise grass pollen sources for each growth season and year. Our hypothesis is that higher correlations indicate a greater possibility of being the pollen sources for a given pollen season.

### 3. Results

#### 3.1 Comparison of filtering grass greenness among multi-resolution grass maps

Fig. 3 displays grass cover areas filtered by the Sentinel-2 grass map (b and f), ALUM (c and g) and DLCD (d and h) around the Campbelltown and Rocklea sites. Fig. 4 shows quantified comparison in the number of grass pixels filtered by each grass map, as well as temporal profiles and correlations between phenocam GCC and filtered grass EVI.

At the Campbelltown site, both the DLCD and ALUM grass map exhibited misclassifications, with certain buildings and roads erroneously labeled as grass. For instance, the ALUM grass map included a substantial portion of a building located southwest of the pollen trap (the red point in Fig. 3). The DLCD grass map misclassified buildings and roads, located north of the pollen trap, as grass covers (Fig. 3d). Conversely, the Sentinel-2 grass map accurately identified these areas as non-grass features, correctly delineating grass areas such as those situated west of the interchange in the Campbelltown site (Fig. 3b), which were missed by the ALUM and DLCD maps. Likewise, at the Rocklea site, the ALUM grass map incorrectly classified all trees within the golf course, situated east of the Rocklea site, as grasses (Fig. 3g). The DLCD map failed to identify a large grass area located southwest of the Rocklea site (Fig. 3h).

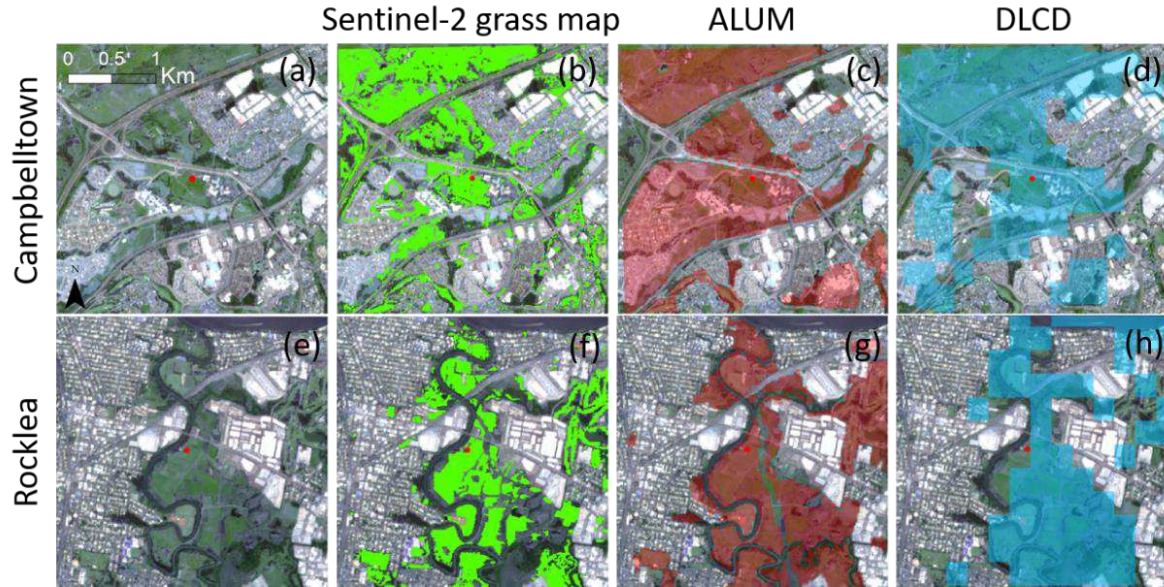


**Fig. 3.** Landscapes and grass areas identified by the Sentinel-2 grass map, ALUM, and DLCD grass maps within the  $3 \times 3 \text{ km}^2$  study areas centered on the Campbelltown (a to d) and Rocklea (e to h) sites. The background images of the landscapes were provided by Google Earth Pro.

The statistical analyses aligned with the visual inspection — the DLCD and ALUM maps identified a significantly higher number of grass pixels compared to the Sentinel-2 grass map at both sites (Fig. 4 a – f). Furthermore, when comparing average values, the grass EVI filtered by the Sentinel-2 grass map was closest to the EVI values obtained from the phenocam footprint (0.77 at the Campbelltown site and 0.67 at the Rocklea site, representing the actual grass greenness around the sites), with values of 0.5 and 0.6 for the Campbelltown and Rocklea sites, respectively (Fig. 4a and 4d).

The time series and correlations between Sentinel-2 EVI (both unfiltered and filtered by grass maps) and phenocam GCC demonstrated that the Sentinel-2 grass map produced optimal grass classification at both sites (Fig. 4 g – l). Specifically, although all grass EVI time series were consistent with the temporal profiles of phenocam GCC, grass EVI filtered by the Sentinel-2 grass map exhibited the largest magnitude due to the exclusion of misclassified grass pixels. Moreover, the Sentinel-2 grass map-filtered grass EVI showed the strongest correlations with phenocam GCC, with  $R^2$  of 0.80 for Campbelltown and 0.41 for Rocklea site (Fig. 4 i and l). Their  $R^2$  and slopes values were closest to the reference values (i.e., correlations between phenocam GCC and Sentinel-2 EVI extracted from the phenocam footprint) at both sites (Fig. 4i and 4l).

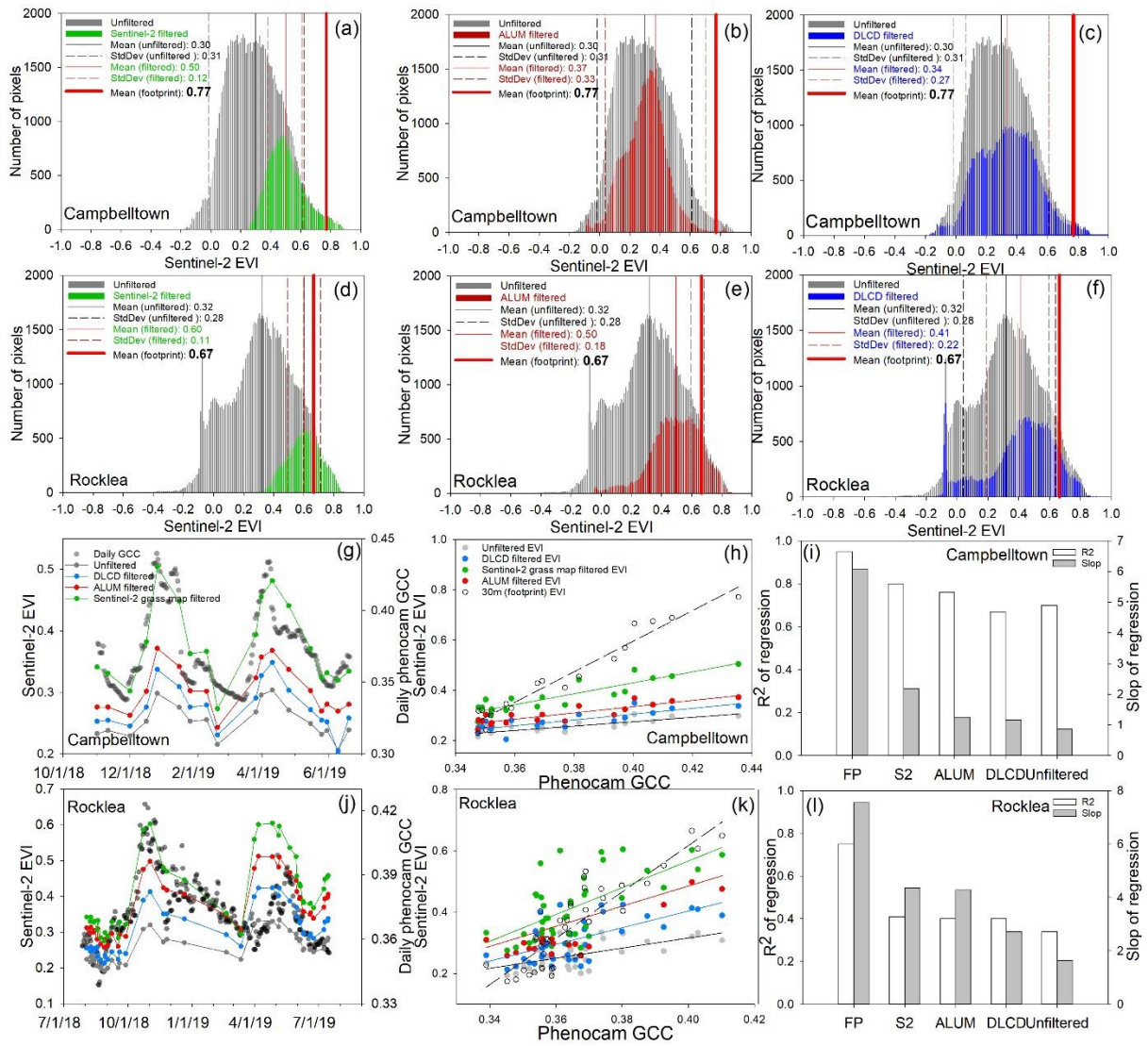


**Fig. 4.** Histogram of pixel numbers from grass map-unfiltered and -filtered Sentinel-2 EVI images ( $3 \times 3 \text{ km}^2$ ) on the greenest day within research period for Campbelltown site (December 26, 2018) and Rocklea site (June 2, 2018) (a – f). The red thick solid line denotes the average Sentinel-2 EVI values extracted from the phenocam ROI footprint ( $3 \times 3$  Sentinel-2 pixels in Fig. 2). It represents the actual grass greenness around each site. Panels g, h, j, and k show the time series and correlations between phenocam GCC and grass EVI filtered by grass maps in Campbelltown and Rocklea sites. Panel i and l summarized the  $R^2$  and slopes of correlations shown in panel h and k, respectively. ‘FP’ represents phenocam ROI footprint, and ‘S2’ represents Sentinel-2 grass map.

### 3.2 Grass greenness dynamics and relationships with grass pollen concentrations around pollen trap station

### 3.2.1 Grass cover fractions filtered by Sentinel-2 grass map at different orientations with extended distances

We used the Sentinel-2 grass map in subsequent analyses due to its superior performance in filtering grass information from heterogeneous landscapes.

Generally, grasses surrounding the Campbelltown pollen trap were predominantly concentrated in the NE1 (northeast 1, 0°–45°), SW1 (southwest 1, 180°–225°), SW2 (southwest 2, 225°–270°), NW1 (northwest 1, 270°–315°), and NW2 (northwest 2, 315°–360°) orientations (Fig. 5a). The grass fractions varied considerably across these different orientations (Fig. 5 b - f). The NW2 orientation exhibited the greatest changes, with grass fractions ranging from 68.39% (within a 2 km radius) to 32.82% (within a 10 km radius). In contrast, the NE2 (northeast 2, 45°–90°) orientation showed the least variation in grass fractions, with grasses uniformly distributed from 2 km (10.64%) to 10 km (10.28%). Among all orientations, the SE1 (southeast 1, 90°–135°) and SW1 directions had the lowest and highest grass fractions within the 10 km radius (3.88% and 50.98%, respectively) (Fig. 5f).

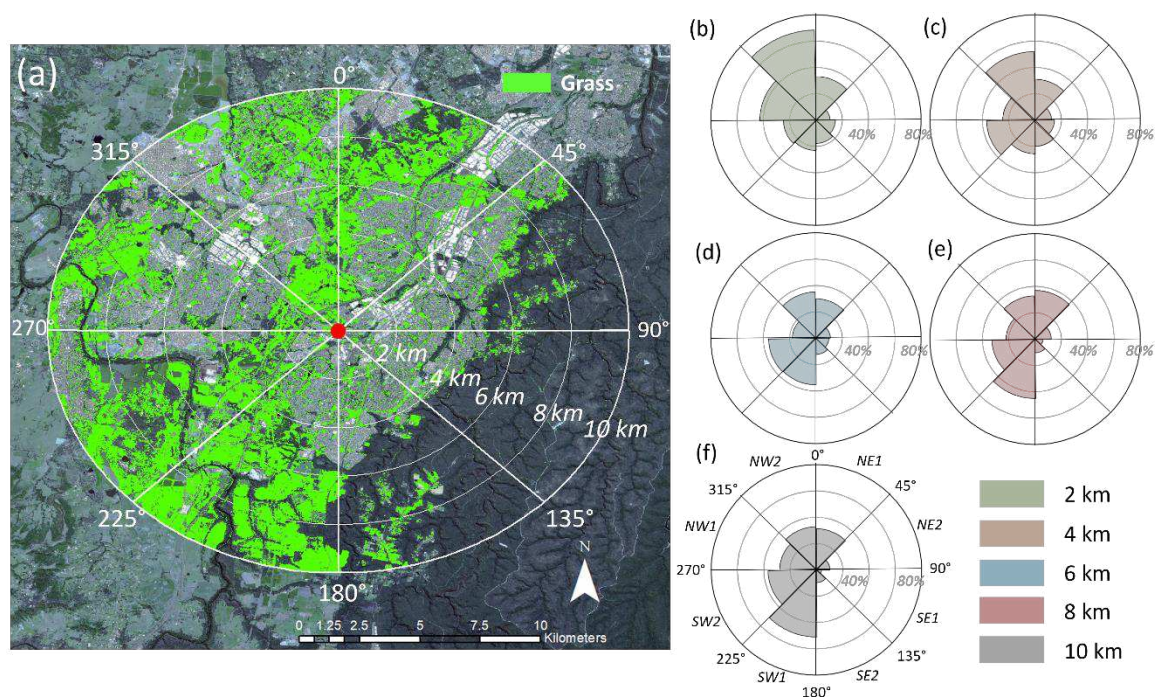


**Fig. 5.** Spatial distribution of Sentinel-2 grass map-filtered grass covers within a region of 10 km radius centered on the Campbelltown pollen trap (a). Grass fractions at different orientations with extended distances (b - f) (i.e., 2 km, 4 km, 6 km, 8 km, and 10 km).

### 3.2.2 Grass EVI and grass pollen concentration time series across orientations and distances

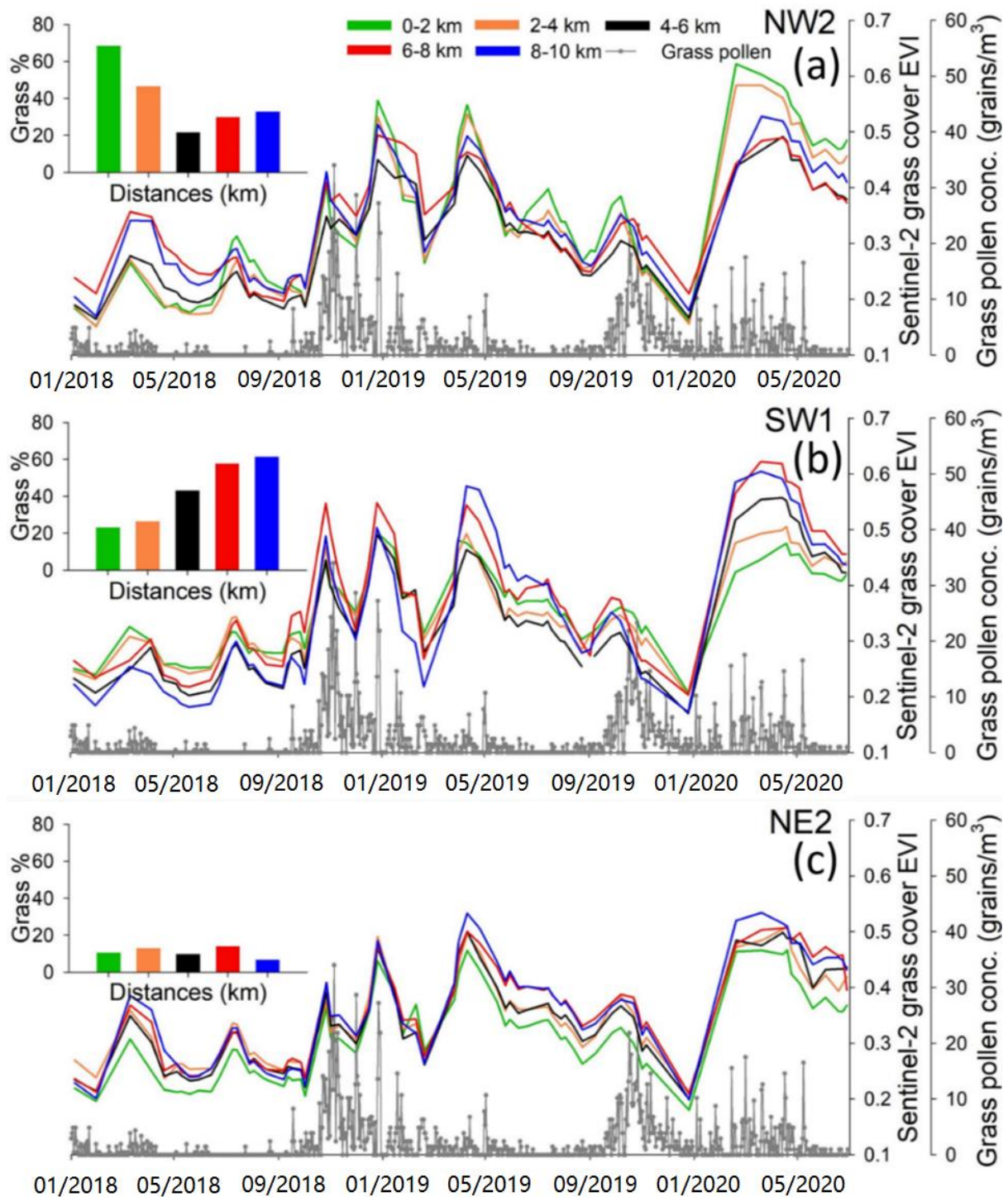
Fig. 6 depicts the time series of in-situ grass pollen concentrations and Sentinel-2 grass EVI averaged from land plots at six distances (0–2 km, 2–4 km, 4–6 km, 6–8 km and 8–10 km) and three selected orientations (NW2, SW1, and NE2). The corresponding grass fractions for each land plot are shown in

the side plots (Fig. 6). Time series of grass EVI and pollen concentrations in other orientations were shown in Fig. A1. While all the grass EVI time series exhibited similar seasonal dynamics, the specific timing of EVI peaks and their magnitudes varied across the land plots.

First, land plots with higher grass fractions did not consistently exhibit larger grass EVI values. Specifically, despite having higher grass fractions, the land plots within the 0–2 km and 2–4 km distance intervals in NW2 displayed lower grass EVI values compared to the 6–8 km and 8–10 km areas from January to June 2018 (Fig. 6a). In the SW1 orientation, land plots with lower grass fractions showed higher grass EVI values during the same period (Fig. 6b). Notably, in the NE2 orientation, the grass EVI values from the 8–10 km area consistently remained higher than those from other land plots throughout the entire growing season, despite this area having lower grass fractions (Fig. 6c).

Second, the grass EVI time series exhibited varied phenology timings (i.e., peak dates) across orientations and distances. In NW2 orientations (Fig. 6a), the grass EVI peak for the 6–8 km area occurred 15 days later than the other EVI peaks during the grass pollen season in October 2019. During the prolonged pollen season in 2020, the grass EVI time series in NW2 displayed peak values on three distinct dates: February 19, 2020, for the 0–2 km and 2–4 km area; March 19, 2020, for the 8–10 km area; and April 14, 2020, for the 4–6 km and 6–8 km areas. In the same pollen season, the grass EVI time series for the 0–2 km and 2–4 km areas reached their peaks on April 19, 2020, in SW1, which was a two-month lag compared to their peaks in NW2 (Fig. 6a and 6b, green and yellow lines).

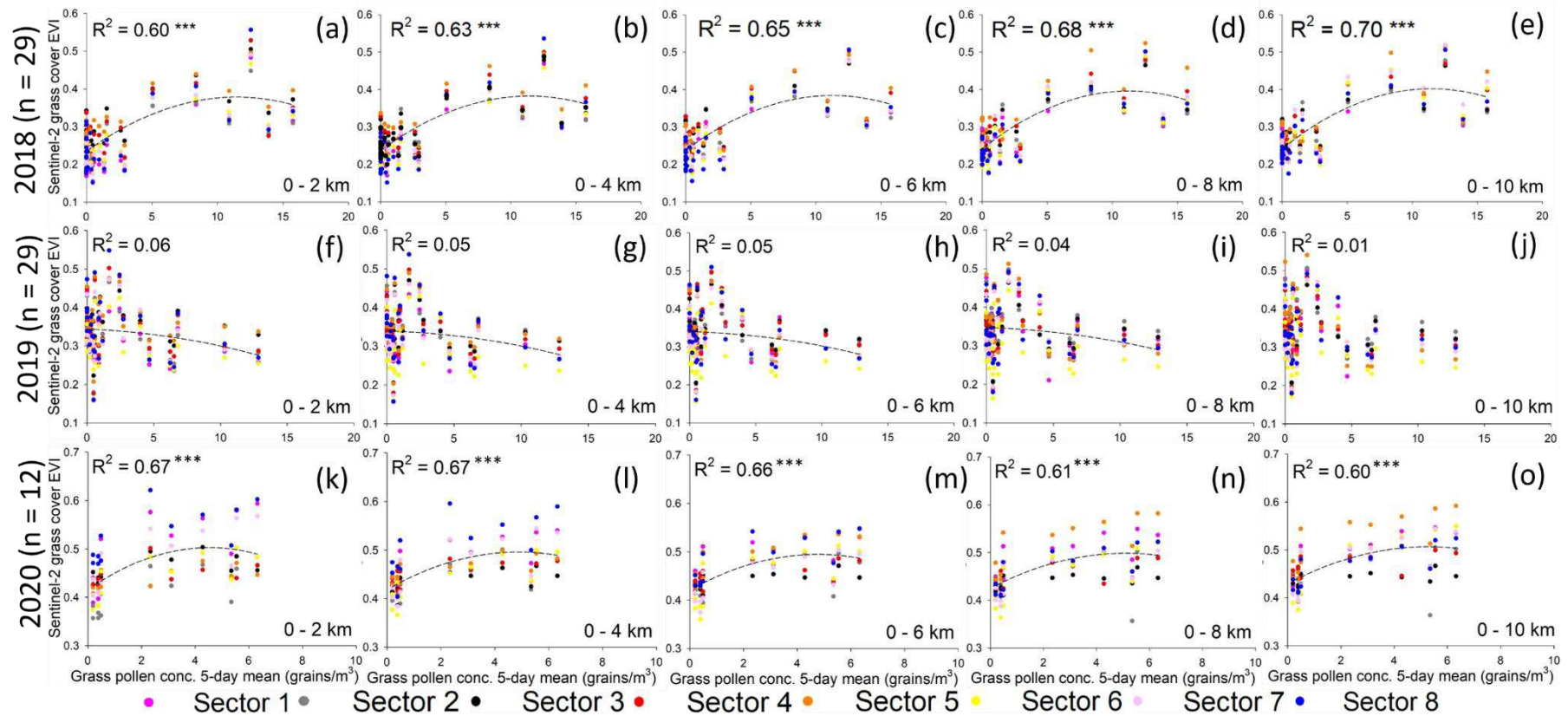
The grass pollen concentrations were notably low in 2018 compared to the levels observed in 2019 and 2020. This discrepancy could be attributed to the presence of moderate grass EVI magnitudes in 2018. It is worth noting that the periods of active grass pollen release were not consistently aligned with the peaks of grass greenness. For example, the main active period of grass pollen in 2019, occurring from October to December, corresponded to secondary peaks of grass greenness rather than the major peaks observed in May 2019. Furthermore, the grass EVI profiles in 2020 displayed a plateau with higher values and several distinct peak dates across distances between February and May, coincided with the extended duration of the grass pollen season in that year. The prolonged presence of green grasses during this period indicates an extended reproductive phase for the grasses, potentially leading to increased grass pollen release.



**Fig. 6.** Time series of in-situ grass pollen concentrations and Sentinel-2 grass cover EVI in (a) NW2 (northwest 2, 315°–365°), (b) SW1 (southwest 1, 180°–225°), and (c) NE2 (northeast 2, 45°–90°) orientations across extended distances surrounding the Campbelltown site from January 2018 to June 2020.

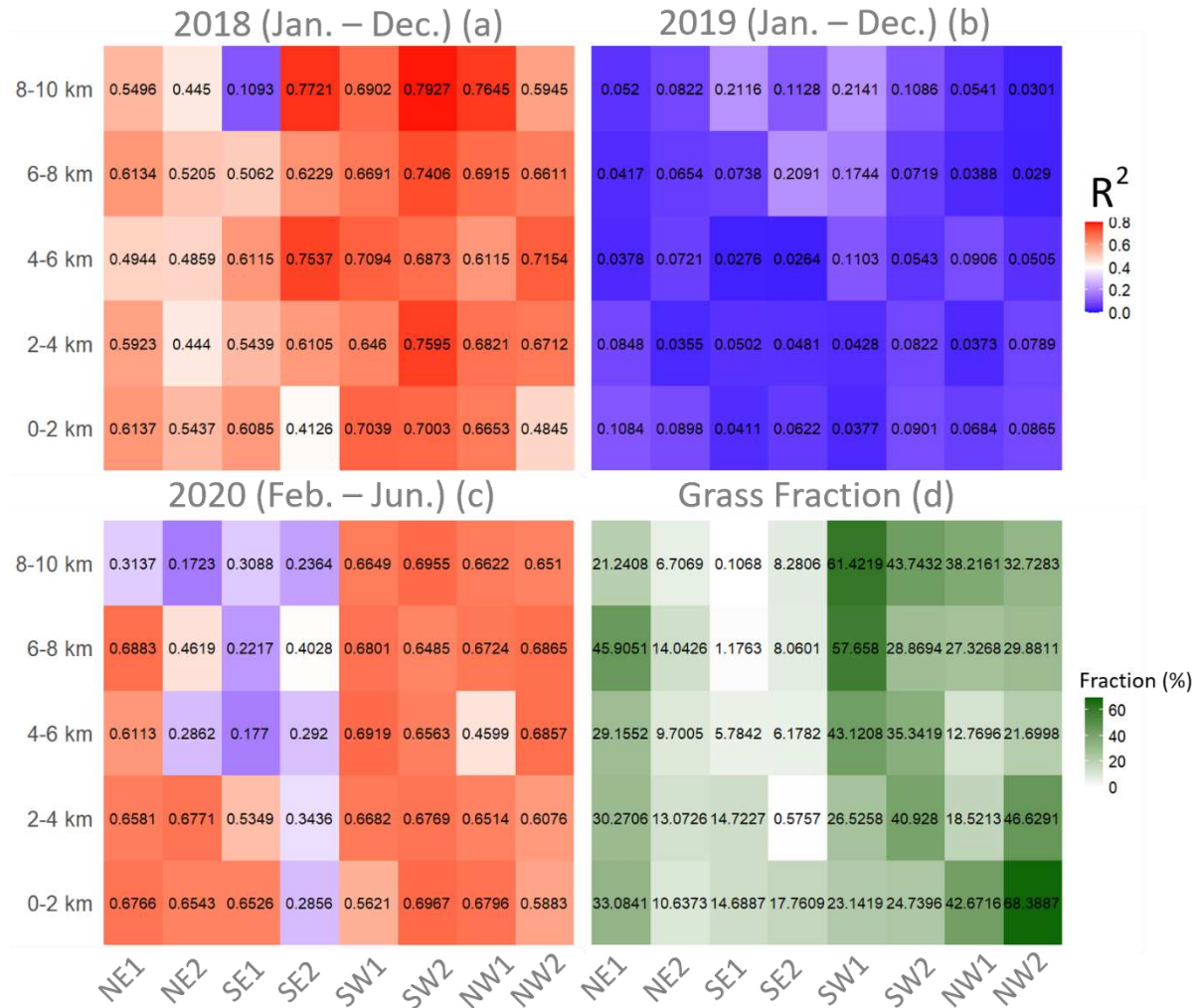
### 3.2.3 Correlations between grass EVI and grass pollen concentrations across orientations and distances

Fig. 7 displays the correlations between time series of five-day mean grass pollen concentrations and grass EVI across increasing distances surrounding the Campbelltown pollen trap. In 2018 (Fig. 7a–e) and 2020 (Fig. 7k–o), strong correlations were observed between grass pollen concentrations and grass EVI at all land plots, with  $R^2$  ranging from 0.60 (0–2 km) to 0.70 (0–10 km) in 2018, and from 0.60 (0–10 km) to 0.67 (0–4 km) in 2020. However, no correlations were observed in 2019 (Fig. 7f–j). It is worth noting that the relationships were nonlinear, with the highest grass pollen concentrations corresponding to lower grass EVI values rather than the highest values (i.e., the greenest grasses). This could be attributed to time lags between the peaks of grass pollen concentrations and the peaks of grass EVI. For example, the grass EVI peak observed around October 2019 preceded the grass pollen peak in November 2019 (Fig. 6).



**Fig. 7.** Correlations between five-day mean grass pollen concentrations and Sentinel-2 grass EVI in land plots with increasing distances (from 2 km to 10 km radius with 2 km interval) surrounding Campbelltown pollen trap in 2018 (a – e), 2019 (f – j), and 2020 (Jan - Jun) (k – o). n = the number of available images each year. Sectors 1 – 8 denote NE1, NE2, SE1, SE2, SW1, SW2, NW1 and NW2 orientations, respectively. \*\*\* denotes correlation significant at  $p = 0.0001$ .

Fig. 8 (a – c) shows the heat map of  $R^2$  from correlations between time series of five-day mean grass pollen concentrations and grass EVI in 40 land plots surrounding the Campbelltown pollen trap. In general, the grass EVI – pollen relationships varied across distances and orientations and exhibited distinct interannual variations. Specifically, stronger relationships were found in the SW1, SW2, NW1, and NW2 directions for both 2018 and 2020. In 2018, as the areas in these directions moved farther apart, the correlations increased, with  $R^2$  values ranging from 0.48 (0-2 km, NW2) to 0.79 (8-10 km SW2). This implied that grass pollen was potentially released by grasses located in more distance regions, explained the  $R^2$  increasing as distance extended shown in Fig. 7 (a – e). In 2020, the correlation remained uniform across distances in these orientations, with  $R^2$  ranging from 0.46 (4-6 km, NW1) to 0.70 (0-2 km, SW2). However, strong agreements between grass greenness and pollen concentrations were found in the SE2 orientation in 2018 with an average  $R^2$  of 0.58, but not in 2020, with an average  $R^2$  of 0.31 (Fig. 8 a and c). Compared to these two years, grass greenness was not associated with grass pollen concentrations in any land plots in 2019 (Fig. 8b).



**Fig. 8.** Heat map of coefficient of determination ( $R^2$ ) for correlations between five-day mean grass pollen concentrations and grass EVI at each land plot in (a) 2018, (b) 2019, and (c) 2020 (Jan - Jun). Panel (d) shows the heat map of the grass fraction in each plot surrounding Campbelltown pollen trap.

Fig. 8d and Fig. 9 display grass fractions and their correlations with the  $R^2$  between grass pollen and grass EVI across 40 land plots (shown in Fig. 8a–c). Upon initial visual inspection (Fig. 8), land plots with lower grass fractions in NE2, SE1, and SE2 (4–10 km) corresponded to weaker grass pollen – EVI correlations in 2020 (Fig. 8c). However, this pattern was not observed in 2018 (Fig. 8a). For example, the grass pollen – EVI  $R^2$  value in land plot (8-10 km, SE2) was as high as 0.77 in 2018, despite a grass fraction of only 8.28%. Furthermore, higher grass fractions were not consistently correlated with significant grass pollen – EVI correlations, e.g., land plot in 0-2 km, NW2. The quantitative analysis shown in Fig. 9 aligned with visual inspection findings. In 2018, grass fraction showed a weak relationship with the grass pollen – EVI  $R^2$  values (Fig. 9a), indicating that a higher grass presence in a

given area did not necessarily correspond to a greater likelihood of being a pollen source. Conversely, in 2020, although the grass fraction positively correlated with grass pollen – EVI relationships, the agreements between grass pollen and EVI did not increase after the grass fraction reached approximately 30% (Fig. 9b). Our results suggest that grass fraction is not the primary factor in understanding grass pollen dynamics.

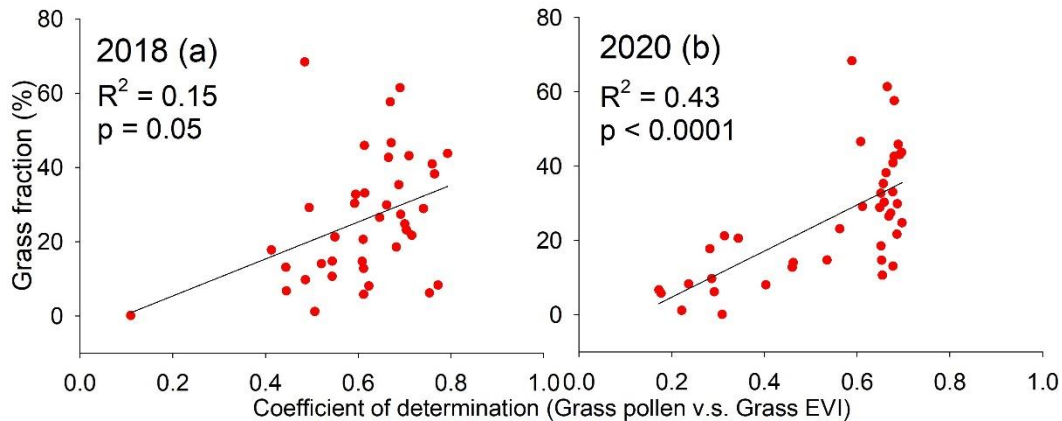


**Fig. 9.** Relationships between grass fractions (Fig. 8d) and coefficients of determination ( $R^2$ ) of grass pollen against grass EVI (Fig. 8 a – c) in 40 land plots surrounding the Campbelltown site for (a) 2018 and (b) 2020 (Jan – Jun).

### 3.3 Intra- and inter-annual variations in spatial distributions of grass pollen sources

Fig. 10 illustrates the variations in pixel-wise spatial distributions of  $R^2$  values of grass pollen – EVI correlations within a  $20 \times 20 \text{ km}^2$  circular region surrounding the Campbelltown pollen trap station for the years 2018, 2019, and 2020. Due to multiple pollen seasons occurring within a single Julian year, we divided each year into several grass pollen seasons based on the time series of grass pollen concentrations and grass EVI. In 2018, there were two pollen seasons (30 January – 20 May 2018 and 7 September – 1 December 2018), three in 2019 (1 December 2018 – 19 February 2019, 26 March – 9 July 2019, and 23 August – 26 December 2019), and one in 2020 (19 February – 28 June 2020). These grass pollen seasons are highlighted by different colors in the time series of grass EVI and are denoted by S1 to S6 in Fig. 10.

Generally, the greenness of the grass surrounding the pollen trap showed better agreements with in-situ grass pollen concentrations in 2018 (S1 and S2) than in 2019 (S3, S4, and S5) and 2020 (S6). The grass pollen concentrations in 2018 was more likely to have originated from the entire research region compared to 2019 and 2020. In 2018, almost all the grasses served as pollen sources in S2 (with uniformly high  $R^2$ , Fig. 10c), whereas only a few orientations contributed grass pollen to S1 (Fig. 10b). For example, grass greenness in the SW2, NW1, and NW2 directions significantly correlated with pollen concentrations in

S2 but not in S1. This might be attributed to the grass species in these three directions predominantly pollinating around October, not March. Also, this indicates that the grass pollen sources varied between different pollen seasons within the same year. Regarding the S3, S4, and S5 in 2019, only a few grass plots acted as grass pollen sources for S5. Furthermore, despite both S2 and S5 occurring from October to January (i.e., the Australian spring), there were significantly fewer pollen sources for S5 compared to S2. This indicates that the grass pollen sources varied between different years, even for similar grass pollen seasons. Similarly, in the autumn pollen season of 2020 (S6), grass plots in five directions were observed as potential grass pollen sources, in contrast to the autumn pollen seasons in 2019 (S3 and S4). Overall, the spatial distribution of grass pollen sources varied across pollen seasons and years.

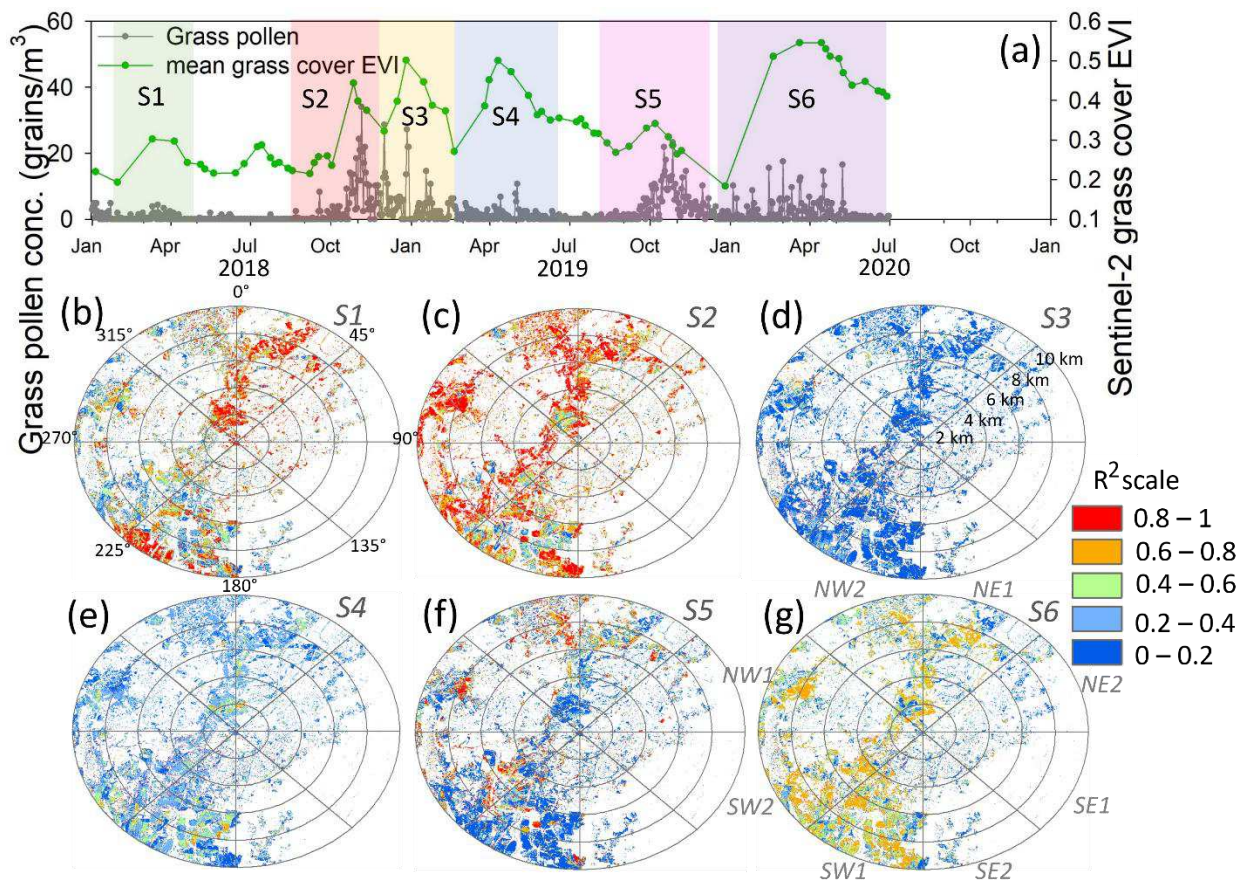


**Fig. 10.** Pixel-wise spatial distribution of coefficient of determination ( $R^2$ ) between five-day mean grass pollen concentrations and Sentinel-2 grass EVI in a  $20 \times 20 \text{ km}^2$  circular region surrounding Campbelltown pollen trap station. The panel (a) shows the time series of Sentinel-2 grass EVI along with daily grass pollen concentrations. Grass pollen seasons were highlighted by different colors. Panels (b) to (g) denote grass pollen seasons 1 to 6 (i.e., S1 – S6), respectively. Regions with white colors in panel (b) to (g) denote non-grass classes according to the Sentinel-2 grass map.

## 4. Discussion

### 4.1 Differences in grass fractions derived from grass maps with multi-resolutions

Plant species used for ornamental and recreational purposes in urban landscapes, such as parks, gardens, tree alignments, and open green spaces, are a major cause of pollen allergies among the local population (Cariñanos et al., 2014). However, accurately describing the spatial distributions of grasses and monitoring the dynamics of grass greenness in urban areas remain challenged. This is mainly due to the use of land cover products with coarse resolutions ( $>10$  m), which are commonly employed to extract grass information from urban landscapes. Although high-resolution images captured by commercial satellites (Dixon et al., 2021) and unmanned aerial vehicles (UAVs) (Guo et al., 2018) offer a promising opportunity to identify grass distributions in urban areas, they are not suitable for large-scale applications at national or continental levels.

In this study, we compared the effectiveness of Sentinel-2 image-derived grass map (10 m) with commonly used land cover product, DLCD (250 m) and ALUM (50 m), in identifying grass distributions in an urban landscape. Our results demonstrated that the Sentinel-2 grass map exhibited promising potential in accurately delineating grass areas, thus enabling a more precise characterization of urban grass greenness. This advanced classification performance of the Sentinel-2 grass map proved valuable in informing the spatial distribution of grass pollen sources. Specifically, Fig. 3 illustrates that both the DLCD and ALUM products mistakenly identify non-grass features as grass due to their coarse resolutions. Consequently, the grass EVI filtered by DLCD and ALUM exhibited weaker correlations with grass phenocam GCC compared to those filtered by the Sentinel-2 grass map (Fig. 4). It is worth noting that, despite the ALUM grass map having a 50 m resolution, its performance was only comparable to that of the DLCD grass map (250 m). This could be attributed to ALUM being designed as a land use map, intended to depict how people utilize the landscape. Although some classes in ALUM include areas with grass cover, it is inevitable that non-grass features, such as trees surrounding golf courses and buildings near recreational lawns, may still be included in the ALUM grass map. In contrast, the Sentinel-2 grass map outperforms coarse resolution maps by accurately delineating grass areas within heterogeneous urban landscapes. This notable performance gives us confidence in using the Sentinel-2 grass map as the foundation (base map) for mapping potential grass pollen sources in the subsequent analyses.

### 4.2 Variations in grass greenness time series and their relationships with grass pollen concentrations across distances and orientations

Grass fractions distinctly varied across distances and orientations in 40 land plots surrounding the Campbelltown pollen trap station (Fig. 5). Despite this, grass EVI averaged from these land plots exhibited consistent temporal patterns throughout the entire study period, with only slight variations in the timing of EVI peaks (Fig. 6 and Fig. A1). On the other hand, the magnitude of grass EVI around peak timings varied significantly and was related to grass fractions, indicating that higher grass fractions corresponded to higher magnitudes of grass EVI. Interestingly, some land plots with larger grass fractions exhibited lower magnitudes of grass EVI from January to May 2018 (Fig. 6a and 6b). This observation might be attributed to the different responses to precipitation between C3 (cool-season grasses) and C4 (subtropical or summer-flowering grasses) species. Previous studies have indicated that aridity can favor the persistence of C4 vegetation under temperature conditions that would otherwise lead to C3 dominance (Cabido et al., 2008). During the summer-autumn months of 2018 (January to May in Australia), precipitation levels were lower compared to those in 2019 and 2020, with monthly totals of 121.2 mm, 225 mm, and 276.6 mm, respectively (Fig. 11). The aridity during this period suppressed the growth of C3 vegetation, which is likely to be predominant in land plots with high grass fractions (Fig. 6), resulting in reduced greenness magnitudes during these arid summer-autumn months in 2018. As precipitation increased in 2019 and 2020, C3 species began to dominate again, leading to an increase in their greenness magnitudes.

The relationships between grass pollen concentrations and grass EVI significantly varied among land plots and years (Fig. 7 and Fig. 8). According to our hypothesis, land plots with higher grass fractions are often expected to have a greater likelihood of releasing grass pollen. Consequently, it is anticipated that the grass EVI in these land plots would show stronger agreements with grass pollen concentrations, as reflected by higher  $R^2$  values. However, our results did not align with this hypothesis. In 2020 (Fig. 9b), correlations between grass EVI and pollen concentrations did not continually increase beyond ~30% grass cover. Furthermore, in 2018 (Fig. 9a), grass EVI derived from some land plots with small grass fractions exhibited stronger correlations with grass pollen concentrations. These findings suggest that while grass fraction plays a role, it appears to act as a secondary control in the grass EVI – pollen correlations.

#### 4.3 Seasonal and inter-annual variations in spatial distributions of grass pollen sources

In this study, we mapped grass pollen sources using correlations between grass pollen and EVI with the Sentinel-2 grass map in a  $20 \times 20$  km<sup>2</sup> circular area around the Campbelltown pollen trap station in Sydney. The grass surrounding the pollen station exhibited six EVI peaks from January 2018 to June 2020, corresponding to periods of grass pollen activities (Fig. 10a). These grass pollen seasons can be categorized into two groups: summer-autumn seasons (S1, S4, and S6) and spring-summer seasons (S2 and S5), represented by red and blue colors in Fig. 11, respectively. The presence of both C3 and C4

grasses in the Sydney region (Hattersley, 1983; Xie et al., 2022) offers a possible explanation for the occurrence of multiple peaks in grass EVI and pollen concentrations within a year, as well as their seasonal and inter-annual variations. We hypothesize that the summer-autumn seasons are associated with C4-dominated grasslands, while the spring-summer seasons are associated with C3-dominated grasslands.

Regarding the summer-autumn pollen season (S1, S4, and S6) associated with C4 grasses (highlighted in red in Fig. 11), their grass pollen sources exhibited differences in spatial distribution and quantities. As previously discussed (section 4.2), lower precipitation favors the growth of C4 grasses while causing browning in C3 grasses. This suggests that C4-dominated grasslands near the pollen trap station (NW2 within a 4 km radius; NE1, NE2, SE1, and SW1) primarily contribute pollen in S1. In contrast, SW2 and NW1 also contributed pollen in S6, possibly due to frequent and heavy precipitation during this season, which likely favored the growth of both C3 and C4 grasses, resulting in a significant increase in grass EVI (Fig. 11). Furthermore, to compensate for competitive disadvantages with C4 grasses, C3 grasses have been shown to flower earlier and have a longer reproductive period (Atkinson et al., 2016; Munson and Long, 2017). Therefore, it is possible that both C4- and C3-dominated grasslands contributed to pollen in S6, leading to an extended pollen season. In the case of the S4 (Fig. 10e), only a small amount of grass was associated with pollen activities compared to S1 and S6. This could be because during S4, although grass greenness increased, grass did not release pollen, resulting in low grass pollen concentrations captured by the pollen station. Another possibility is that grass did release pollen during S4, but it was not captured by the pollen trap due to meteorological variables, such as increased relative humidity, which typically hinders airborne pollen transport (Rojo et al., 2015). This assumption is supported by the heavy rainfall that occurred at the beginning of the S4 season (Fig. 11).

Typically, C3 grasses in Australia reach their greenness peak in late October to early November. However, previous research has shown that high rainfall can lead to a C3 greenness peak occurring in January (Watson et al., 2019). This aligns with our findings, as we observed an EVI peak in January 2019 following heavy precipitation in December 2018. Given this, the anomalous EVI peak in S3, driven by rainfall, might not have significant pollination ability. Consequently, grass pollen concentrations decreased while grass greenness increased, and only small portions of grass were associated with pollen dynamics in S3 (Fig. 10c). In the case of the other two spring pollen seasons (S2 and S5) associated with C3 grasses (highlighted in blue in Fig. 11), the smaller amounts of pollen sources and lower grass EVI in S5 can be partly attributed to lower precipitation compared to S2.

Overall, the variations in the distribution of grass pollen sources among seasons are not solely associated with grass phenology (e.g., EVI peaks) but also with other factors such as precipitation and relative humidity. In further studies, it is worthwhile to delve into the effect of meteorological variables on pollen

emission and dispersal when using satellite-based remote sensing to understand the aerobiology of grass pollen.

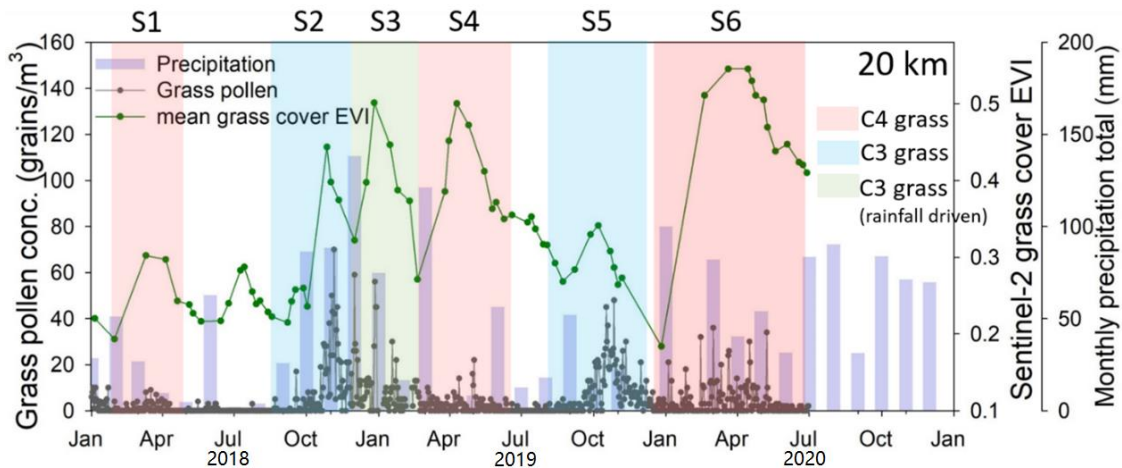


**Fig. 11.** Time series of monthly precipitation total and mean grass Sentinel-2 EVI averaged from the  $20 \times 20 \text{ km}^2$  circular area around Campbelltown site from 2018 to 2020. Summer-autumn pollen seasons associated with C4 grasses are highlighted by red colors. Blue and green colors highlight spring-summer pollen seasons associated with C3 grasses.

## 5. Conclusion

In this study, we have demonstrated the potential of Sentinel-2 data with 10 m resolution to enhance the identification of grassland areas within heterogeneous urban landscapes and to inform the spatial distribution of grass pollen sources. By leveraging Sentinel-2 data's capabilities in capturing both the timing of grass phenology and the geospatial distributions of grass, we have achieved promising results that open new possibilities for mapping grass pollen sources and understanding their seasonal patterns at regional and continental scales.

Based on our findings and subsequent discussions, we have arrived at three key conclusions:

- (1) The 10 m Sentinel-2 grass map proved effective in excluding non-grass features misidentified as grass in coarse grass maps (ALUM and DLCD). Consequently, the grass EVI derived from the Sentinel-2 grass map demonstrated a better correlation with in-situ phenocam observations of grass phenology. This underscores the advanced capability of the Sentinel-2 grass map to filter out grass-related information from heterogeneous urban landscapes.
- (2) The temporal dynamics of grass EVI obtained from the Sentinel-2 grass map, and their relationships with grass pollen concentrations, significantly varied across different land plots with varied grass

fractions. However, grass fraction was not the primary factor controlling the grass EVI – pollen correlations, contrary to our initial expectation.

(3) The Campbelltown pollen station exhibited significant seasonal and inter-annual variability in grass pollen sources in terms of their spatial distributions and amounts. To accurately interpret these variations, further attention should be directed towards understanding the influence of meteorological factors on the phenology of C3 and C4 grass functional types, as well as on the emission and transport of pollen.

## Acknowledgements

This work was funded by the University of Technology Sydney (UTS) International Research Scholarship and President's Scholarship, as an in-kind contribution to an Australian Research Council (ARC) Discovery Project (DP170101630) led by Distinguished Professor Alfredo Huete (University of Technology Sydney), Professor Janet Davies (Queensland University of Technology) and Associate Professor Paul Beggs (Macquarie University). We thank Dr. Abolfazl Abdollahi and Professor Biswajeet Pradhan for generating Sentinel-2 grass map. Additional support was provided by the Victorian Department of Health and Human Services Victorian Thunderstorm Asthma Pollen Surveillance (VicTAPS) program led by the Bureau of Meteorology. We thank the Queensland Department of Science and Environment Air Quality Environmental Monitoring Team for their support and access to the phenocam site at Rocklea.

## References

- Abdollahi, A., Liu, Y., Pradhan, B., Huete, A., Dikshit, A., Nguyen Tran, N., 2022. Short-time-series grassland mapping using Sentinel-2 imagery and deep learning-based architecture. *The Egyptian Journal of Remote Sensing and Space Science* 25, 673–685.  
<https://doi.org/10.1016/j.ejrs.2022.06.002>
- Asher, M.I., Montefort, S., Björkstén, B., Lai, C.K., Strachan, D.P., Weiland, S.K., Williams, H., 2006. Worldwide time trends in the prevalence of symptoms of asthma, allergic rhinoconjunctivitis, and eczema in childhood: ISAAC Phases One and Three repeat multicountry cross-sectional surveys. *The Lancet* 368, 733–743.  
[https://doi.org/10.1016/S0140-6736\(06\)69283-0](https://doi.org/10.1016/S0140-6736(06)69283-0)
- Atkinson, R.R.L., Mockford, E.J., Bennett, C., Christin, P.-A., Spriggs, E.L., Freckleton, R.P., Thompson, K., Rees, M., Osborne, C.P., 2016. C4 photosynthesis boosts growth by altering physiology, allocation and size. *Nature Plants* 2, 16038.  
<https://doi.org/10.1038/nplants.2016.38>
- Beaumont, L., Hartenthaler, T., Keatley, M., Chambers, L., 2015. Shifting time: recent changes to the phenology of Australian species. *Clim. Res.* 63, 203–214.  
<https://doi.org/10.3354/cr01294>
- Beggs, P.J., Katelaris, C.H., Medek, D., Johnston, F.H., Burton, P.K., Campbell, B., Jaggard, A.K., Vicendese, D., Bowman, D.M.J.S., Godwin, I., Huete, A.R., Erbas, B., Green, B.J., Newnham, R.M., Newbigin, E., Haberle, S.G., Davies, J.M., 2015. Differences in grass pollen allergen exposure across Australia. *Australian and New Zealand Journal of Public Health* 39, 51–55. <https://doi.org/10.1111/1753-6405.12325>
- Brennan, G.L., Potter, C., De Vere, N., Griffith, G.W., Skjøth, C.A., Osborne, N.J., Wheeler, B.W., McInnes, R.N., Clewlow, Y., Barber, A., Hanlon, H.M., Hegarty, M., Jones, L., Kurganskiy, A., Rowney, F.M., Armitage, C., Adams-Groom, B., Ford, C.R., Petch, G.M., The PollerGEN Consortium, Elliot, A., Frisk, C.A., Neilson, R., Potter, S., Rafiq, A.M., Roy, D.B., Selby, K., Steinberg, N., Creer, S., 2019. Temperate airborne grass pollen defined by spatio-temporal shifts in community composition. *Nat Ecol Evol* 3, 750–754.  
<https://doi.org/10.1038/s41559-019-0849-7>

- Cabido, M., Pons, E., Cantero, J.J., Lewis, J.P., Anton, A., 2007. Photosynthetic pathway variation among C 4 grasses along a precipitation gradient in Argentina. *J Biogeography* 0, 070727014816001. <https://doi.org/10.1111/j.1365-2699.2007.01760.x>
- Cariñanos, P., Casares-Porcel, M., Quesada-Rubio, J.-M., 2014. Estimating the allergenic potential of urban green spaces: A case-study in Granada, Spain. *Landscape and Urban Planning* 123, 134–144. <https://doi.org/10.1016/j.landurbplan.2013.12.009>
- Cariñanos, P., Sánchez-Mesa, J.A., Prieto-Baena, J.C., Lopez, A., Guerra, F., Moreno, C., Domínguez, E., Galan, C., 2002. Pollen allergy related to the area of residence in the city of Córdoba, south-west Spain. *J. Environ. Monit.* 4, 734–738. <https://doi.org/10.1039/B205595C>
- Chen, Jun, Chen, Jin, Liao, A., Cao, X., Chen, L., Chen, X., He, C., Han, G., Peng, S., Lu, M., Zhang, W., Tong, X., Mills, J., 2015. Global land cover mapping at 30m resolution: A POK-based operational approach. *ISPRS Journal of Photogrammetry and Remote Sensing* 103, 7–27. <https://doi.org/10.1016/j.isprsjprs.2014.09.002>
- Clark, M.L., 2017. Comparison of simulated hyperspectral HypsIRI and multispectral Landsat 8 and Sentinel-2 imagery for multi-seasonal, regional land-cover mapping. *Remote Sensing of Environment* 200, 311–325. <https://doi.org/10.1016/j.rse.2017.08.028>
- Darrow, L.A., Hess, J., Rogers, C.A., Tolbert, P.E., Klein, M., Sarnat, S.E., 2012. Ambient pollen concentrations and emergency department visits for asthma and wheeze. *Journal of Allergy and Clinical Immunology* 130, 630-638.e4. <https://doi.org/10.1016/j.jaci.2012.06.020>
- Davies, J.M., Beggs, P.J., Medek, D.E., Newnham, R.M., Erbas, B., Thibaudon, M., Katelaris, C.H., Haberle, S.G., Newbigin, E.J., Huete, A.R., 2015. Trans-disciplinary research in synthesis of grass pollen aerobiology and its importance for respiratory health in Australasia. *Science of The Total Environment* 534, 85–96. <https://doi.org/10.1016/j.scitotenv.2015.04.001>
- De Linares, C., Díaz De La Guardia, C., Nieto Lugalde, D., Alba, F., 2010. Airborne Study of Grass Allergen (Lol p 1) in Different-Sized Particles. *Int Arch Allergy Immunol* 152, 49–57. <https://doi.org/10.1159/000260083>
- Denize, J., Hubert-Moy, L., Corgne, S., Betbeder, J., Pottier, E., 2018. Identification of Winter Land Use in Temperate Agricultural Landscapes based on Sentinel-1 and 2 Times-Series,

- in: IGARSS 2018 - 2018 IEEE International Geoscience and Remote Sensing Symposium. IEEE, Valencia, pp. 8271–8274. <https://doi.org/10.1109/IGARSS.2018.8517673>
- Descals, A., Verger, A., Yin, G., Peñuelas, J., 2020. Improved Estimates of Arctic Land Surface Phenology Using Sentinel-2 Time Series. *Remote Sensing* 12, 3738. <https://doi.org/10.3390/rs12223738>
- Devadas, R., Huete, A.R., Vicendese, D., Erbas, B., Beggs, P.J., Medek, D., Haberle, S.G., Newnham, R.M., Johnston, F.H., Jaggard, A.K., Campbell, B., Burton, P.K., Katelaris, C.H., Newbigin, E., Thibaudon, M., Davies, J.M., 2018. Dynamic ecological observations from satellites inform aerobiology of allergenic grass pollen. *Science of The Total Environment* 633, 441–451. <https://doi.org/10.1016/j.scitotenv.2018.03.191>
- Dixon, D.J., Callow, J.N., Duncan, J.M.A., Setterfield, S.A., Pauli, N., 2021. Satellite prediction of forest flowering phenology. *Remote Sensing of Environment* 255, 112197. <https://doi.org/10.1016/j.rse.2020.112197>
- Emmerson, K.M., Silver, J.D., Newbigin, E., Lampugnani, E.R., Suphioglu, C., Wain, A., Ebert, E., 2019. Development and evaluation of pollen source methodologies for the Victorian Grass Pollen Emissions Module VGPEM1.0. *Geosci. Model Dev.* 12, 2195–2214. <https://doi.org/10.5194/gmd-12-2195-2019>
- Erbas, B., Dharmage, S.C., Tang, M.L.K., Akram, M., Allen, K.J., Vicendese, D., Davies, J.M., Hyndman, R.J., Newbigin, E.J., Taylor, P.E., Bardin, P.G., Abramson, M.J., 2015. Do human rhinovirus infections and food allergy modify grass pollen–induced asthma hospital admissions in children? *Journal of Allergy and Clinical Immunology* 136, 1118–1120.e2. <https://doi.org/10.1016/j.jaci.2015.04.030>
- Fragoso-Campón, L., Quirós, E., Mora, J., Gutiérrez, J.A., Durán-Barroso, P., 2018. Accuracy Enhancement for Land Cover Classification Using LiDAR and Multitemporal Sentinel 2 Images in a Forested Watershed, in: *Environment, Green Technology, and Engineering International Conference*. MDPI, p. 1280. <https://doi.org/10.3390/proceedings2201280>
- Gómez-Giráldez, P.J., Pérez-Palazón, M.J., Polo, M.J., González-Dugo, M.P., 2020. Monitoring Grass Phenology and Hydrological Dynamics of an Oak–Grass Savanna Ecosystem Using Sentinel-2 and Terrestrial Photography. *Remote Sensing* 12, 600. <https://doi.org/10.3390/rs12040600>

- Guo, W., Zheng, B., Potgieter, A.B., Diot, J., Watanabe, K., Noshita, K., Jordan, D.R., Wang, X., Watson, J., Ninomiya, S., Chapman, S.C., 2018. Aerial Imagery Analysis – Quantifying Appearance and Number of Sorghum Heads for Applications in Breeding and Agronomy. *Front. Plant Sci.* 9, 1544. <https://doi.org/10.3389/fpls.2018.01544>
- Haberle, S.G., Bowman, D.M.J.S., Newnham, R.M., Johnston, F.H., Beggs, P.J., Buters, J., Campbell, B., Erbas, B., Godwin, I., Green, B.J., Huete, A., Jaggard, A.K., Medek, D., Murray, F., Newbiggin, E., Thibaudon, M., Vicendese, D., Williamson, G.J., Davies, J.M., 2014. The Macroecology of Airborne Pollen in Australian and New Zealand Urban Areas. *PLoS ONE* 9, e97925. <https://doi.org/10.1371/journal.pone.0097925>
- Hattersley, P.W., 1983. The distribution of C3 and C4 grasses in Australia in relation to climate. *Oecologia* 57, 113–128. <https://doi.org/10.1007/BF00379569>
- Huete, A., Didan, K., Miura, T., Rodriguez, E.P., Gao, X., Ferreira, L.G., 2002. Overview of the radiometric and biophysical performance of the MODIS vegetation indices. *Remote Sensing of Environment* 83, 195–213. [https://doi.org/10.1016/S0034-4257\(02\)00096-2](https://doi.org/10.1016/S0034-4257(02)00096-2)
- Intelligent information and database systems, 2019. . Springer Berlin Heidelberg, New York, NY.
- Karlsen, S.R., Ramfjord, H., Høgda, K.A., Johansen, B., Danks, F.S., Brobakk, T.E., 2009. A satellite-based map of onset of birch (*Betula*) flowering in Norway. *Aerobiologia* 25, 15–25. <https://doi.org/10.1007/s10453-008-9105-3>
- Khwarahm, N.R., Dash, J., Skjøth, C.A., Newnham, R.M., Adams-Groom, B., Head, K., Caulton, E., Atkinson, P.M., 2017. Mapping the birch and grass pollen seasons in the UK using satellite sensor time-series. *Science of The Total Environment* 578, 586–600. <https://doi.org/10.1016/j.scitotenv.2016.11.004>
- Köppen, W., 2011. The thermal zones of the Earth according to the duration of hot, moderate and cold periods and to the impact of heat on the organic world. *metz* 20, 351–360. <https://doi.org/10.1127/0941-2948/2011/105>
- Längkvist, M., Kiselev, A., Alirezaie, M., Loutfi, A., 2016. Classification and Segmentation of Satellite Orthoimagery Using Convolutional Neural Networks. *Remote Sensing* 8, 329. <https://doi.org/10.3390/rs8040329>

- Linkosalo, T., 2000. Mutual regularity of spring phenology of some boreal tree species: predicting with other species and phenological models. *Can. J. For. Res.* 30, 667–673. <https://doi.org/10.1139/x99-243>
- Linkosalo, T., 1999. Regularities and patterns in the spring phenology of some boreal trees. *Silva Fenn.* 33. <https://doi.org/10.14214/sf.647>
- Louis, J., Pflug, B., Main-Knorn, M., Debaecker, V., Mueller-Wilm, U., Iannone, R.Q., Giuseppe Cadau, E., Boccia, V., Gascon, F., 2019. Sentinel-2 Global Surface Reflectance Level-2a Product Generated with Sen2Cor, in: *IGARSS 2019 - 2019 IEEE International Geoscience and Remote Sensing Symposium*. IEEE, Yokohama, Japan, pp. 8522–8525. <https://doi.org/10.1109/IGARSS.2019.8898540>
- Ma, X., Huete, A., Moran, S., Ponce-Campos, G., Eamus, D., 2015. Abrupt shifts in phenology and vegetation productivity under climate extremes: ECOSYSTEM FUNCTIONAL RESPONSE TO DROUGHT. *J. Geophys. Res. Biogeosci.* 120, 2036–2052. <https://doi.org/10.1002/2015JG003144>
- Mazzia, V., Khaliq, A., Chiaberge, M., 2019. Improvement in Land Cover and Crop Classification based on Temporal Features Learning from Sentinel-2 Data Using Recurrent-Convolutional Neural Network (R-CNN). *Applied Sciences* 10, 238. <https://doi.org/10.3390/app10010238>
- McInnes, R.N., Hemming, D., Burgess, P., Lyndsay, D., Osborne, N.J., Skjøth, C.A., Thomas, S., Vardoulakis, S., 2017. Mapping allergenic pollen vegetation in UK to study environmental exposure and human health. *Science of The Total Environment* 599–600, 483–499. <https://doi.org/10.1016/j.scitotenv.2017.04.136>
- Medek, D.E., Beggs, P.J., Erbas, B., Jaggard, A.K., Campbell, B.C., Vicendese, D., Johnston, F.H., Godwin, I., Huete, A.R., Green, B.J., Burton, P.K., Bowman, D.M.J.S., Newnham, R.M., Katelaris, C.H., Haberle, S.G., Newbiggin, E., Davies, J.M., 2016. Regional and seasonal variation in airborne grass pollen levels between cities of Australia and New Zealand. *Aerobiologia* 32, 289–302. <https://doi.org/10.1007/s10453-015-9399-x>
- Miranda, E., Mutiara, A.B., Wibowo, W.C., 2019. Forest Classification Method Based on Convolutional Neural Networks and Sentinel-2 Satellite Imagery. *IJFIS* 19, 272–282. <https://doi.org/10.5391/IJFIS.2019.19.4.272>

- Munson, S.M., Long, A.L., 2017. Climate drives shifts in grass reproductive phenology across the western USA. *New Phytol* 213, 1945–1955. <https://doi.org/10.1111/nph.14327>
- Newnham, R.M., Sparks, T.H., Skjøth, C.A., Head, K., Adams-Groom, B., Smith, M., 2013. Pollen season and climate: Is the timing of birch pollen release in the UK approaching its limit? *Int J Biometeorol* 57, 391–400. <https://doi.org/10.1007/s00484-012-0563-5>
- Newson, R.B., Van Ree, R., Forsberg, B., Janson, C., Lötvall, J., Dahlén, S.-E., Toskala, E.M., Baelum, J., Brožek, G.M., Kasper, L., Kowalski, M.L., Howarth, P.H., Fokkens, W.J., Bachert, C., Keil, T., Krämer, U., Bislimovska, J., Gjomarkaj, M., Loureiro, C., Burney, P.G.J., Jarvis, D., 2014. Geographical variation in the prevalence of sensitization to common aeroallergens in adults: the GA 2 LEN survey. *Allergy* 69, 643–651. <https://doi.org/10.1111/all.12397>
- Nguyen, H.T.T., Doan, T.M., Tomppo, E., McRoberts, R.E., 2020. Land Use/Land Cover Mapping Using Multitemporal Sentinel-2 Imagery and Four Classification Methods—A Case Study from Dak Nong, Vietnam. *Remote Sensing* 12, 1367. <https://doi.org/10.3390/rs12091367>
- Pelletier, C., Webb, G.I., Petitjean, F., 2019. Deep Learning for the Classification of Sentinel-2 Image Time Series, in: *IGARSS 2019 - 2019 IEEE International Geoscience and Remote Sensing Symposium*. IEEE, Yokohama, Japan, pp. 461–464. <https://doi.org/10.1109/IGARSS.2019.8900123>
- Phiri, D., Simwanda, M., Salekin, S., Nyirenda, V., Murayama, Y., Ranagalage, M., 2020. Sentinel-2 Data for Land Cover/Use Mapping: A Review. *Remote Sensing* 12, 2291. <https://doi.org/10.3390/rs12142291>
- Qiu, C., Schmitt, M., Geiß, C., Chen, T.-H.K., Zhu, X.X., 2020. A framework for large-scale mapping of human settlement extent from Sentinel-2 images via fully convolutional neural networks. *ISPRS Journal of Photogrammetry and Remote Sensing* 163, 152–170. <https://doi.org/10.1016/j.isprsjprs.2020.01.028>
- Rapinel, S., Mony, C., Lecoq, L., Clément, B., Thomas, A., Hubert-Moy, L., 2019. Evaluation of Sentinel-2 time-series for mapping floodplain grassland plant communities. *Remote Sensing of Environment* 223, 115–129. <https://doi.org/10.1016/j.rse.2019.01.018>

- Rojo, J., Rapp, A., Lara, B., Fernández-González, F., Pérez-Badia, R., 2015. Effect of land uses and wind direction on the contribution of local sources to airborne pollen. *Science of The Total Environment* 538, 672–682. <https://doi.org/10.1016/j.scitotenv.2015.08.074>
- Segal-Rozenhaimer, M., Li, A., Das, K., Chirayath, V., 2020. Cloud detection algorithm for multi-modal satellite imagery using convolutional neural-networks (CNN). *Remote Sensing of Environment* 237, 111446. <https://doi.org/10.1016/j.rse.2019.111446>
- Skjøth, C.A., Ørby, P.V., Becker, T., Geels, C., Schlünssen, V., Sigsgaard, T., Bønløkke, J.H., Sommer, J., Søgaaard, P., Hertel, O., 2013. Identifying urban sources as cause of elevated grass pollen concentrations using GIS and remote sensing. *Biogeosciences* 10, 541–554. <https://doi.org/10.5194/bg-10-541-2013>
- Verstraeten, W.W., Kouznetsov, R., Hoebeke, L., Bruffaerts, N., Sofiev, M., Delcloo, A.W., 2021. Modelling grass pollen levels in Belgium. *Science of The Total Environment* 753, 141903. <https://doi.org/10.1016/j.scitotenv.2020.141903>
- Vrieling, A., Meroni, M., Darvishzadeh, R., Skidmore, A.K., Wang, T., Zurita-Milla, R., Oosterbeek, K., O'Connor, B., Paganini, M., 2018. Vegetation phenology from Sentinel-2 and field cameras for a Dutch barrier island. *Remote Sensing of Environment* 215, 517–529. <https://doi.org/10.1016/j.rse.2018.03.014>
- Wang, L.L., Bornert, M., Héripré, E., Chanchole, S., Pouya, A., Halphen, B., 2015. The Mechanisms of Deformation and Damage of Mudstones: A Micro-scale Study Combining ESEM and DIC. *Rock Mech Rock Eng* 48, 1913–1926. <https://doi.org/10.1007/s00603-014-0670-1>
- Watson, C.J., Restrepo-Coupe, N., Huete, A.R., 2019. Multi-Scale Phenology of Temperate Grasslands: Improving Monitoring and Management With Near-Surface Phenocams. *Front. Environ. Sci.* 7, 14. <https://doi.org/10.3389/fenvs.2019.00014>
- Xie, Q., Huete, A., Hall, C.C., Medlyn, B.E., Power, S.A., Davies, J.M., Medek, D.E., Beggs, P.J., 2022. Satellite-observed shifts in C3/C4 abundance in Australian grasslands are associated with rainfall patterns. *Remote Sensing of Environment* 273, 112983. <https://doi.org/10.1016/j.rse.2022.112983>
- Zink, K., Pauling, A., Rotach, M.W., Vogel, H., Kaufmann, P., Clot, B., 2013. EMPOL 1.0: a new parameterization of pollen emission in numerical weather prediction models. *Geosci. Model Dev.* 6, 1961–1975. <https://doi.org/10.5194/gmd-6-1961-2013>

Zink, K., Vogel, H., Vogel, B., Magyar, D., Kottmeier, C., 2012. Modeling the dispersion of *Ambrosia artemisiifolia* L. pollen with the model system COSMO-ART. *Int J Biometeorol* 56, 669–680. <https://doi.org/10.1007/s00484-011-0468-8>

## Appendix

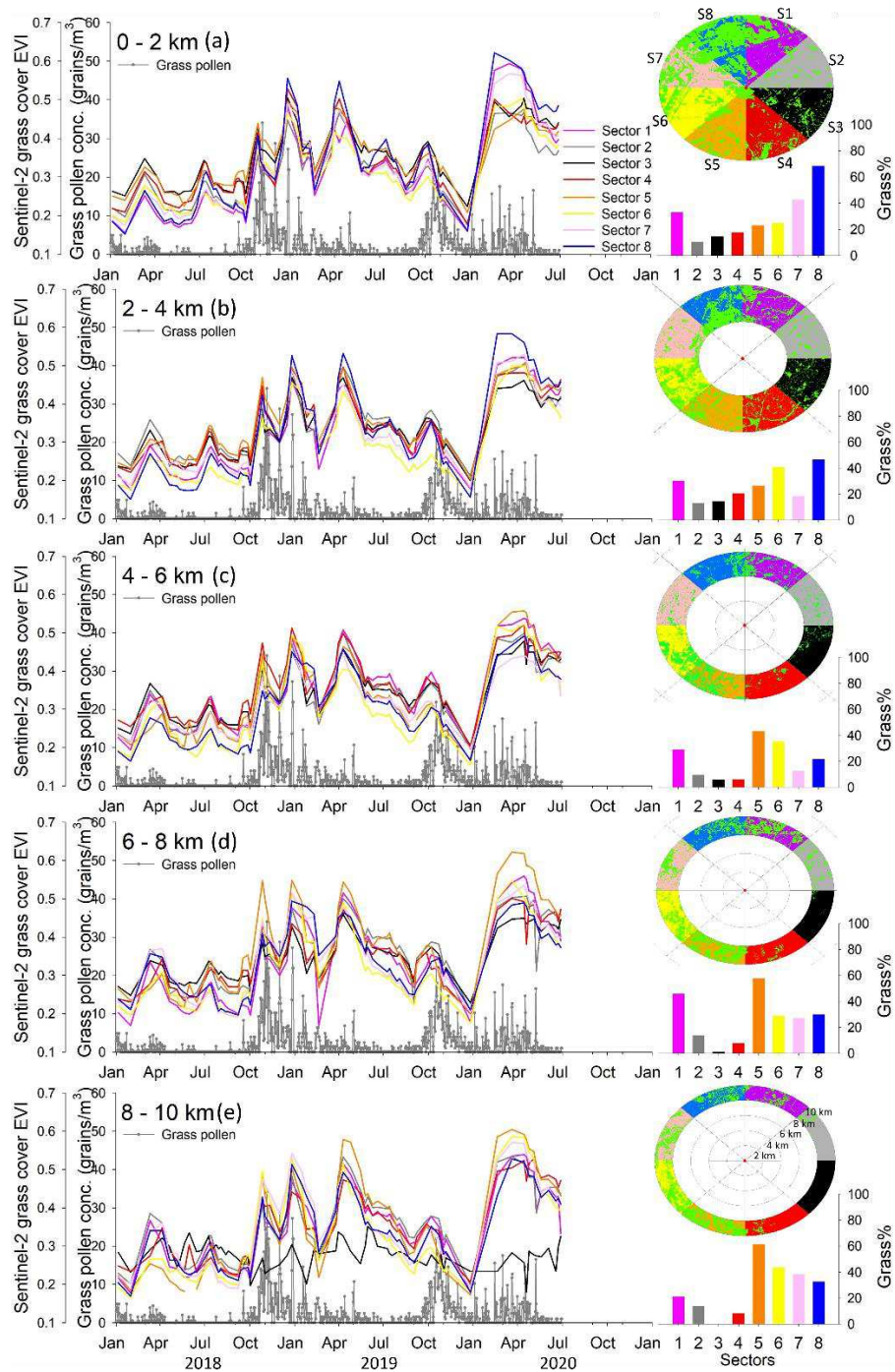


**Fig. A1.** Time series of grass pollen concentrations and Sentinel-2 grass EVI averaged from 40 land plots surrounding the Campbelltown pollen trap station, which showed in top-right panels, from January 2018 to June 2020. The bottom-right panels show grass fractions in land plots. Sectors 1 to 8 respectively corresponded to areas of  $0^\circ - 45^\circ$  to  $315^\circ - 365^\circ$  in Fig. 5.